

Improved Presentation Attack Detection Using Image Decomposition

Shlok Kumar Mishra ^{1,2*} Kuntal Sengupta ², Wen-Sheng Chu ²,
 Max Horowitz-Gelb ², Sofien Bouaziz ², David Jacobs¹
¹University of Maryland, College Park, ²Google Research,
 {shlok, dwj}@cs.umd.edu

Abstract

Presentation attack detection (PAD) is a critical component in secure face authentication. We present a PAD algorithm to distinguish face spoofs generated by a photograph of a subject from live images. Our method uses an image decomposition network to extract albedo and normal. The domain gap between the real and spoof face images leads to easily identifiable differences, especially between the recovered albedo maps. We enhance this domain gap by retraining existing methods using supervised contrastive loss. We present empirical and theoretical analysis that demonstrates that contrast and lighting effects can play a significant role in PAD; these show up particularly in the recovered albedo. Finally, we demonstrate that by combining all of these methods we achieve state-of-the-art results on both intra-dataset testing for CelebA-Spoof, OULU, CASIA-SURF datasets and inter-dataset setting on SiW, CASIA-MFSD, Replay-Attack and MSU-MFSD datasets.

1. Introduction

Recently, face recognition has been widely adopted for applications such as phone unlock and mobile payments. During a secure face authentication session, a presentation attack detection (PAD) system is tasked with distinguishing between a real human face and a face in a presentation attack instrument (PAI) in front of the camera. Examples of PAI includes printed paper attacks, replay attacks on displays, etc. Commercial PAD methods rely on a depth sensor and active near-infrared illumination to increase the robustness of the system. This makes these methods unsuitable for low-cost mobile devices with a single RGB camera.

In recent years several handcrafted features [6, 7, 23, 32, 33, 67] and deep learning-based approaches [4, 14, 16, 21, 35, 52, 54, 67] have been designed for PAD. Recent methods have predicted depth signals from a single RGB im-

age [57, 58, 65, 66] using PRNet [12]. However, the reconstructed depth often looks similar for the real and the spoof images. Hence these methods hardcode the depth of spoof image to be zero. We on the other hand argue that face albedo is better suited for PAD. This is demonstrated in Figure 1 where the surface-normal (normal) and the depth maps are visually similar for real images and for spoof images. The albedo map is visually different, motivating us to primarily condition our classification network on the face albedo. In contrast to depth we don't need to hardcode the albedo for real and spoof images as they are distinctively different. Also, estimating albedo doesn't require a expensive depth sensor hardware, hence making it suitable for low-cost mobile devices.

Our emphasis on albedo is motivated by differences in contrast and lighting between real and spoof images, affecting the recovered albedo. We show empirically that real and spoof images have significantly different contrast. In fact, removing this contrast difference results in a drastic drop in spoof detection performance by the state of the art approaches such as Central Difference Convolution(CDCN) [65]. Theoretically, we show that lighting differences between real and spoof images also create effects that will show up in recovered albedo.

These differences allow us to take advantage of the domain gap between real images and spoof images [19, 65]. To verify this, we train the image decomposition network with only real images. This creates a domain gap when classifying spoof images. We use supervised contrastive losses [22] to further increase this domain gap. Supervised contrastive loss is a generalization of triplet losses that can work on large batches of negative samples. In PAD, we apply contrastive learning on real and spoof images. This forces the network to push the feature embeddings of real and spoof images far from each other, accentuating the difference between the real and the spoof domains.

We propose the IDCL architecture (Fig 2) to assess the value of albedo and normal. Initially, we pretrain a network using supervised contrastive loss. We use this as the initialization point for the RGB backbone in our IDCL ar-

* Work was done when Shlok was interning at Google Research.

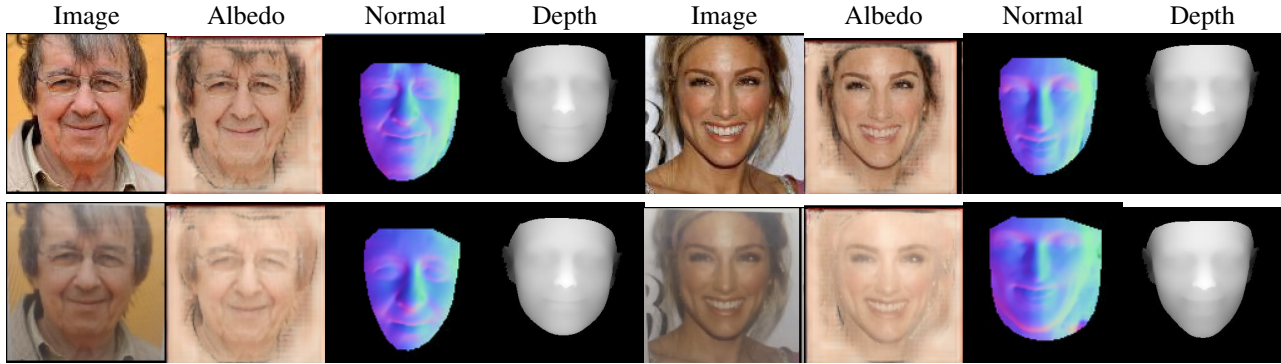


Figure 1: Live images (*top row*) and spoof images (*bottom row*) show similar reconstructed depth maps and surface normal. Albedo, on the other hand, looks different for spoof images and live images. Albedo helps in capturing the contrast difference resulting from different lighting interactions that happen on the spoof images. Here, we propose to use albedo as additional cue for detecting spoofs in addition to using depth maps.



Figure 2: IDCL network: We propose IDCL network to use image decomposition [34] for the task of PAD. We have three different networks corresponding to three different modalities i.e. RGB, albedo and normal. Empirically and visually, the albedo performs on-par in detecting spoofs compared to normal and depth maps.

chitecture. Next, we add surface normal and albedo signals as input to the IDCL network and train it to classify spoofs. From our experiments on CASIA-SURF [61] and OULU-NPU [8], we observe that albedo is a better cue and has more impact on performance as compared to the surface normal. The primary motive of IDCL architecture is to understand the effects of albedo and normal for spoof detection and not to improve upon state-of-the-art methods.

To achieve state-of-the-art results we add supervised contrastive loss initialization and albedo as a cue to various methods on seven different datasets. We start by adding contrastive loss and an albedo component to AENet [56]. AENet has state-of-the-art results on the CeleBA-Spoof dataset, which is the largest public dataset available for spoof detection. Our methods outperform AENet [56], and we achieve state-of-the-art results on CeleBA-Spoof. We also add supervised contrastive loss initialization and albedo components on top of CDCN [65] and on top of the winners of Chalearn Challenge[1] and achieve state-of-the-art results on OULU-NPU [8] and CAISA-SURF[61] as well. We also show state-of-the-art results on intra-dataset protocol on SiW dataset [63] and on CASIA-MFSD [63], Replay-Attack [10] and MSU-MFSD [49] datasets.

Finally, we provide a theoretical analysis of the effect of lighting on spoof images. Spoof images can be affected by the interplay between two lighting conditions. Consider, for example, the case of a paper attack in which spoofs are captured using mobile phones. There is one lighting condition when the original image is captured, and another one when the spoof picture is captured with the phone. In Sec 5.3 we show that this combination of lighting can create effects on the face not generally produced by a single lighting condition. Specifically, we show that this interplay introduces new, higher frequency artifacts that can corrupt the albedo, and can be used to identify spoofs.

Our contributions can be summarized as follows:

1. We study the impact of using albedo maps, normal and depth information for the task of PAD. Through qualitative and quantitative experiments, we verify that albedo is the stronger cue for detecting spoofs.
2. To the best of our knowledge, our approach is the first to show the use of supervised contrastive loss for PAD. Supervised contrastive loss helps generate better initialization points that transfer well for spoof detection.
3. We achieve state-of-the-art results on OULU-NPU, CeleBA-Spoof, SiW dataset, CASIA-MFSD, Replay-

Attack and MSU-MFSD datasets. We also demonstrate that by adding albedo as conditioning to various state-of-art methods, their performance can be improved.

4. Through theoretical analysis and experiments, we demonstrate that contrast and lighting effects can play a significant role in spoof detection.

2. Related Work

Presentation Attack Detection (PAD): Traditionally PAD has been solved for RGB images by using various local descriptors and features such as HOG features [23], SIFT features [32], or SURF [7]. For video spoofing datasets, where input are videos, various methods have been proposed that capture dynamic features such as texture [23], motion [40] and eye blinks [31]. Recently deep learning-based methods have been proposed to identify spoofs. Here, a convolutional neural network (CNN) backbone is trained to extract features that can be used to identify spoofs [20, 35, 59, 60, 65, 66]. A few methods also use depth as a cue to identify spoof images [53, 65]. Our work shows that albedo is a stronger signal to identify spoofs compared to depth or other geometric information extracted from an RGB image; this is a marked departure from these standard methods. Concurrent work [64] uses a similar idea and shows results on Forgery Detection using deviation from the common texture as an important feature. We on the other hand focus on spoof detection and using albedo as a cue.

Image Decomposition: Traditionally geometry estimation methods for faces were based on 3D Morphable models (3DMM) [5, 25, 39, 41–44]. Recently, a few studies have demonstrated the effectiveness of CNN’s to solve the problem of geometry estimation [15, 27, 38, 39, 42, 45]. Depth estimated using PRNet [12] has also been used as a cue to detect spoofs [19, 35, 65]. In our work, we propose to use image decomposition to estimate albedo. We use SharinGAN [34], which is based on SFSNet [38] to extract albedo features and surface normals from images and use them as signals to detect spoofs.

Contrastive Learning: Contrastive learning-based methods have been recently gaining popularity for self-supervised learning [9, 17, 18, 51] and supervised learning [22]. We use supervised contrastive learning to increase the domain gap between spoof images and real images, which gives us a better initialization point for our networks.

3. Our method

Recent methods have taken advantage of the domain gap between real and face images to identify spoofs [3, 19]. Potential reasons for this gap include color distortion, display artifacts, presenting artifacts and imaging artifacts as discussed by Face De-Spoofing [3]. We show that domain gap can also be caused by the contrast difference between the

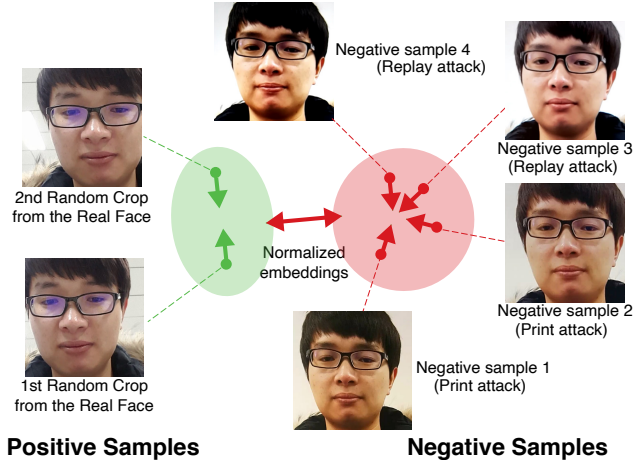


Figure 3: We use supervised contrastive learning to increase the domain gap between spoof images and live images. In supervised contrastive learning the negative sample comes from different class from the positive class. If the positive sample is from the real image, the negative sample would be from a spoof image and vice-versa. Hence a contrastive learning approach will push real images and spoof images away from each other, thus increasing the domain gap.

real and the spoof images and also by the presence of a linear gradient on the images which may cause these networks to learn sub-optimal representations. We discuss these issues in more detail in Section 5. Now we discuss our proposed approach, which amplifies the domain gap.

3.1. Amplifying the domain gap with image decomposition:

To calculate geometric features from real images, we use SharinGAN [34], which computes normal, albedo and lighting. SharinGAN [34] is based on SFSNet [38] with additional components that reduce the domain gap between synthetic and real training data. Next, we use the normal and albedo computed by SharinGAN as input to our network, along with the original RGB. We train three networks independently, one for each modality, i.e RGB, albedo and normal and fuse them in later layers, as shown in Fig. 2.

Amplifying the domain gap in image decomposition: Domain gaps between training and testing data have been a long-standing issue in Computer Vision [2, 29, 30, 46]. However, this gap can be advantageous in our case, if it can be used to cause reconstruction methods to perform differently on real and spoof images. To achieve this, we train SharinGAN [34] using only real images from the Spoofing dataset. By doing this, the network will not have seen the spoof images during training, and hence the network will produce more accurate image decomposition for real images as compared to spoof images. We call this network

SharinGAN-Real and its impact is shown in Table 2.

3.2. Increasing the domain gap with contrastive loss

Traditionally, methods such as adversarial loss have been used to create latent features that have the same distribution for both domains. We instead use the contrastive loss to widen the gap between these distributions.

Contrastive methods are generalizations of triplet losses [22] and have been shown to work very well in Supervised and Self-Supervised Learning (SSL) methods [17, 51]. We will first discuss the details of supervised contrastive loss and then its application to the spoof detection problem.

Supervised contrastive loss: Supervised contrastive loss [22] imposes a constraint that normalized embeddings from the same class are closer than the ones from different classes. Contrastive losses consist of two “opposing forces”: for a given anchor point, the first force pulls the anchor closer to positive examples in the representation space, and the second force pushes the anchor farther away from negative points. In the supervised contrastive loss, negative samples come from different classes than the positive class.

In our case, the positive samples are augmentations of the same face and negative samples would be any spoof image. We perform augmentation by taking two random crops from the same face. Hence the contrastive training method will force the network to push the representations of real images and spoof images far from each other, thus increasing the domain gap between real and spoof images.

IDCL: Image Decomposition and Contrastive Loss

Now we discuss how we combine the image decomposition method SharinGAN [34] and supervised contrastive loss. Our proposed architecture IDCL (image decomposition and contrastive loss) as shown in Fig 2 has three branches for the three modalities, RGB, albedo and normal. First, we pre-train a randomly initialized neural network by supervised contrastive loss on the RGB images. We use this pretrained network and initialize the RGB branch of the IDCL network from this pretrained point. Next, we use the output of the SharinGAN (i.e albedo and normal components), and feed these components and the RGB frames as inputs to three different branches in our IDCL network. We also aggregate information from all the preceding layers in their final layers as was done in [1]. Note that we don’t set the depth map of spoof image to be zero which is a common practice in state-of-the-art methods; instead we use the output of PRNet [12] directly for both real and spoof images. We then train our IDCL network in an end to end fashion using all these three modalities. More details of the the IDCL architecture can be found in supplementary.

4. Results

We start by briefly describing the datasets used in our experiments. Then we show that using supervised contrastive

losses can help in achieving better initialization and can boost performance by a fair margin. We then present results supporting our hypothesis that albedo is a strong cue for detecting spoofs. We demonstrate this across two datasets, CASIA-SURF [61] and OULU-NPU [8]. Then we show the impact of the domain gap by only using real images while training image decomposition methods. Finally we verify that adding albedo as a signal to OULU-NPU, CASIA-SURF and CelebA-spoof helps us in achieving state of the art results on these datasets.

4.1. Datasets

CelebA-Spoof [56]: CelebA-Spoof is a recently released dataset and the biggest open source spoof corpus. CelebA-Spoof [56] has 625,537 samples of 10,117 subjects, and is significantly bigger than other Anti-Spoofing datasets. In total there are 8 scenes (2 environments * 4 illumination conditions) and more than 10 sensors. It also has 10 spoof type annotations and 40 attribute annotations closely following the original CelebA-dataset [67].

OULU-NPU: OULU-NPU is a high quality dataset [8] that contains four protocols to test the generalization capability of anti-spoofing systems.

CASIA-SURF: CASIA-SURF [61] is a large scale dataset with 21,000 videos. Each sample of CASIA-SURF has three modalities (i.e RGB, Depth and NIR).

SiW: SiW dataset is designed for cross-type testing for unseen attacks. We show cross-domain testing results on SiW dataset.

CASIA-MFSD [63], Replay-Attack [10] and MSU-MFSD [49]: CASIA-MFSD [63], Replay-Attack [10] and MSU-MFSD [49] datasets contain low-resolution videos which are used for cross domain testing.

4.2. Results using the IDCL architecture

In this section, we show the results of using image decomposition methods and contrastive learning.

Using contrastive learning: The use of supervised contrastive loss helps in increasing the already existing domain gap between spoof and non-spoof images. To evaluate this we pre-train our network using supervised contrastive learning using only RGB images. Then we use this pre-trained backbone and finetune for the task of spoof classification. We compare our results with an RGB baseline in which we train a randomly initialized network for the task of spoof classification as shown in Table 2 and Table 1. We can see from Table 2 and Table 1 that adding contrastive loss helps in learning better representations. We can see that there is an improvement of around 15.58% on the OULU dataset and 10.21% for the CAISA-SURF dataset as compared to the RGB baseline. Hence, when only using RGB images we can see that pre-training the network with supervised contrastive loss helps in learning better representations.

Table 1: We show results on CASIA-SURF. The first row shows the results of using ground truth depth and NIR information; we can see that this solves the problem quite well. The second row shows the baseline using only RGB frames. Using supervised contrastive loss helps us in achieving 10.21% improvements over the RGB baseline. We can see that after using SharinGAN, we improve by 59.09% over our RGB baseline.

Method	TPR@FPR=10-2	TPR@FPR=10-3	TPR@FPR=10-4
Using RGB/NIR/depth	0.9997	0.9967	0.6850
Using Only RGB	0.4646	0.1299	0.0651
Supervised Contrastive (Ours)	0.5119	0.1676	0.1151
IDCL (Ours)	0.7391	0.3373	0.1126

Table 2: We present the results on OULU-NPU for Protocol 1. We observe that after using SharinGAN we improve by 44% on our RGB baseline. Using supervised contrastive we improve by 15.58% over the RGB baseline.

Method	TPR@FPR=10-2	TPR@FPR=10-3	TPR@FPR=10-4
RGB baseline	0.43	0.05	0.05
RGB with Supervised Contrastive loss	0.53	0.25	0.25
RGB and SharinGAN (using albedo and normal)	0.53	0.24	0.24
RGB and SharinGAN-Real (using albedo and normal)	0.65	0.39	0.39

Using all three modalities: We use a pretrained SharinGAN [34] on CelebA to extract depth and albedo information from images. Next, to accentuate the domain gap we train SharinGAN [34] using only real images from the spoofing datasets. This encourages SharinGAN to make better predictions for real images than for spoof images. We can see the impact of training the network using only real images in Table 2. We can see that using SharinGAN-Real we are able to achieve performance improvements of 50.01% over the RGB only baseline. Hence this shows that training SharinGAN with real images and taking advantage of domain gap helps in learning better representations. We only verify this result for OULU-NPU and not for CASIA-SURF, because the quality of images is too low in CASIA-SURF to retrain image decomposition methods. In the case of CelebA-Spoof, there is no domain gap since SFSNet and SharinGAN have been trained on the CelebA dataset as the real-world dataset. We only illustrate results using normal, since depth maps and normals are principally very similar.

4.3. Ablation study on albedo and normal

IDCL: One of the main hypotheses in our work is that albedo is a better cue for detecting spoofs as compared to depth and surface normals as shown in Fig 1. To exam-

Table 3: Results on CASIA-SURF using albedo, depth and IR information. The metric used is TPR@FPR=threshold.

Method	thr=1e-2	thr=1e-3	thr=1e-4
Baseline[1]	100.0	100.0	.9987
Ours	100.0	100.0	.9998

ine this difference empirically, we perform ablation studies on normals and albedo. To do this, we drop one branch at a time from the IDCL architecture shown in Fig 2. We can see from Table 4 for both datasets dropping albedo results in significant drops in performance(25.8% for CASIA-SURF and 18.8% for OULU) and dropping normal results in a smaller drop in the performance(7.9% for CASIA-SURF and 9.09% for OULU). This suggests that albedo is a stronger cue for detecting spoofs in both the datasets.

4.4. State-of-the-art results using albedo and contrastive loss

In addition to showing that albedo is a useful cue for detecting spoofs, we also show that adding albedo to existing methods can be used to get state-of-the-art results on high-quality datasets like OULU-NPU [8] and large datasets like CelebA-spoof [56] and CASIA-SURF [61]. We also show that adding contrastive loss initialization can help in achieving even better results. To show state-of-the-art results we add an albedo component to the baselines architectures. We follow CDCN [65] for OULU, AENet [56] for CelebA-spoof [56] and build on top of the winners of Chalearn-Challenge [1] for CASIA-SURF. We see that we can improve upon the performance of CDCN [65] across all four OULU protocols, as shown in Table 7. We are also able to improve upon the performance of CelebA [56] as shown in Table 5 and on CASIA-SURF as shown in Table 3. In the case of CASIA-SURF these results are pretty saturated, and there’s little room for improvement. We also show cross-testing results on MSU-MFSD [50], Replay-Attack [11] and CASIA-MFSSD [62] as shown in Table 9. Similarly cross-testing on SiW dataset are shown in Table 8.

Table 4: Ablation results dropping albedo and normal for both datasets. We first removed the normal maps, and we see a performance drop of 7.9% for CASIA-SURF and 9.09% for OULU. Next, we remove the albedo components and we see a more significant drop of 25.8% for CASIA-SURF and 18.8% for OULU. This shows that albedo is a bigger cue, and dropping albedo impacts the performance more than dropping normal.

Method	Dataset	TPR@FPR=10-2	TPR@FPR=10-3	TPR@FPR=10-4
IDCL	OULU	0.65	0.39	0.39
Albedo removed	OULU	0.55	0.31	0.31
Normal removed	OULU	0.60	0.53	0.53
IDCL	CASIA-SURF	0.73	0.33	0.11
Albedo removed	CASIA-SURF	0.57	0.33	0.10
Normal Removed	CASIA-SURF	0.68	0.27	0.10

Table 5: Results on CelebA-Spoof after adding Albedo to AENet [56]. We can see that adding albedo component improves performance over baseline AENet [56]. Supervised contrastive loss initialization helps in improving the results even further as shown in last row.

Method	TPR@FPR=1%	TPR@FPR=0.5%	TPR@FPR=0.1%	APCER	BPCER	ACER
Baseline AENet [56]	98.9	97.8	90.9	4.62	1.09	2.85
Albedo-SharinGAN (Ours)	99.1	98.1	91.2	4.31	0.93	2.62
+ Contrastive Loss (Ours)	99.3	98.4	91.5	3.79	0.81	2.30

5. Analysis

In this section, we discuss contrast cues and theoretical analysis, considering the effect of ambient lighting on spoof images. We show some additional visual analysis which is produced by image decomposition methods in the supplementary material.

5.1. Occlusion based visualization

To better understand our network features, we apply occlusion at different portions of the input image with a grey patch and monitor the classifier output. Green patches in Fig 4 indicates the regions where occlusion leads to a strong drop in activation in the feature map. More activation drop can be observed in the live image than in the spoof image, showing that albedo feature contains more texture information of the live image than of a spoof one.

5.2. Contrast cues

We show that contrast is a significant cue for spoofs in current state-of-the-art datasets [8, 61]. To verify contrast as

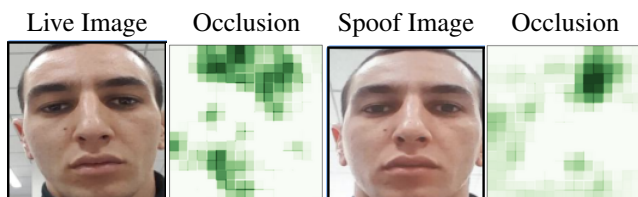


Figure 4: Visualization using occlusion based attribution.

a cue, we first calculated the mean and standard deviation of contrast on the OULU training set for real images and spoof images. We center the images to have zero mean and calculate the root mean square of pixel intensity, i.e. contrast value. For real images, the contrast was 81.64 ± 14.97 , and for spoof images, the contrast was 72.36 ± 13.91 . We observe that there is a significant gap between the contrast of real images and spoof images. To remove contrast as a cue, we perform histogram equalization on the images. Next, we retrained the current state of the art method CDCN [65], and we observe a significant drop in performances in Table 6. This performance drop suggests that contrast as a cue is being used in current systems. Hence we propose to use albedo, which is especially well suited to help us in capturing this contrast difference. Complete table with results on all the protocols is shown in supplementary materials.

5.3. Theoretical analysis of ambient lighting

In this section, we consider the effect of ambient lighting on spoof images. In a photograph of a face, appearance is influenced by the lighting. In PAD, one captures a photograph of an existing photograph. Hence, the spoof image is also affected by a second lighting condition, as the Presentation Attack Instrument (the photograph in this case) itself reflects light. We analyze a simple case to show how this second lighting condition can produce effects that could not have arisen in an original photograph of a face.

It is well-known that an image of a convex Lambertian

Table 6: We show the impact of removing contrast as a cue from spoof detection systems. We can see that after removing contrast, we see a performance drop in spoof detection on CDCN[65]. Hence to capture this contrast cue and other lighting cues, we propose to use albedo to detect spoof images.

Method	Protocol	APCER	BPCER	ACER
CDCN [65]	1	0.4	0.0	0.2
CDCN contrast removed [65]	1	4	3	3.5

Table 7: Results on OULU-NPU [8] on protocols P=1,2,3,4. We add an albedo component to the CDCN [65] architecture and achieve state-of-the-art results. Our experiment is denoted as ‘‘SharinGAN+CDCN’’ as the last row, where we add albedo component from SharinGAN and add it to CDCN [65].

P	Method	APCER	BPCER	ACER
1	FaceDs [21]	1.2	1.7	1.5
1	FAS-TD [48]	2.5	0.0	1.3
1	CDCN++ [65] (Base-line)(Reproduced)	1.5	1.2	1.3
1	NAS-FAS[55]	0.4	0.0	0.2
1	SharinGAN+CDCN	0.8	0.7	0.7
1	+ Contrastive Loss	0.7	0.6	0.6
2	GRADIANT [7]	3.1	1.9	2.5
2	STASN [52]	4.2	0.3	2.2
2	CDCN++ [65] (Base-line)(Reproduced)	2.0	1.6	1.8
2	NAS-FAS[55]	1.5	0.8	1.2
2	SharinGAN+CDCN	1.5	1.4	1.4
2	+ Contrastive Loss	1.3	1.1	1.2
3	FaceDs [21]	4.0±1.8	3.8±1.2	3.6±1.6
3	STASN [52]	4.7±3.9	0.9±1.2	2.8±1.5
3	CDCN++ [65] (Base-line)(Reproduced)	2.3±1.5	2.5±1.2	2.3±0.7
3	NAS-FAS[55]	2.1±1.3	1.4±1.1	1.7±0.6
3	SharinGAN+CDCN	2±1.5	2.1±1.1	2.0±0.7
3	+ Contrastive Loss	1.7±1.4	1.8±1.1	1.7±0.7
4	FAS-TD [48]	14.2±8.7	4.2±3.8	9.2±3.4
4	STASN [52]	6.7±10.6	8.3±8.4	7.5±4.7
4	CDCN++ [65] (Base-line)(Reproduced)	4.5±3.4	6.3±4.9	5.3±2.9
3	NAS-FAS[55]	4.2±5.3	1.7±2.6	2.9±2.8
4	SharinGAN+CDCN	4.0±1.6	6.0±4.8	5.0±2.8
4	+ Contrastive Loss	3.4±1.5	5.5±4.4	4.5±2.7

Table 8: Results of intra testing on three protocols of SiW.

Prot.	Method	APCER(%)	BPCER(%)	ACER(%)
1	CDCN++	0.07	0.17	0.12
	CDCN + SharinGAN(Ours)	0.04	0.12	0.6
2	CDCN++	0.00±0.00	0.09±0.10	0.04±0.05
	CDCN + SharinGAN(Ours)	0.00±0.00	0.09±0.10	0.04±0.05
3	CDCN++	1.97±0.33	1.77±0.10	1.90±0.15
	CDCN + SharinGAN(Ours)	1.43±0.30	1.54±0.10	1.58±0.15

object is primarily determined by the low-frequency components of light, hardly reflecting any of the higher frequency components [36, 37]. Several previous works have applied this model to faces with excellent results, indicating that this is a good model in spite of the non-convex, non-Lambertian aspects of human faces [24, 26, 37, 47]. When a photograph of a face is imaged, the light impinging on the photograph scales its intensities. Below we show that in general, this can introduce higher frequency effects that were not present in the original photo.

5.3.1 Analysis of a simple case

In this section, we analyze the simplified case of a photo of a white Lambertian unit sphere. Then we discuss the relevance of this result to our approach.

We first consider distant, environment map lighting. Distant light can be represented as intensity as a function of direction. We denote this function as $r(\hat{u})$, where \hat{u} is a unit vector indicating direction. With Lambertian reflectance, the irradiance, that is, the intensity of light reflected by a point on the sphere is:

$$i(\hat{v}) = \int_{\hat{u}} r(\hat{u}) \max(0, \hat{u} \cdot \hat{v}) d\hat{u}$$

This is essentially convolution with a cosine filter that is clipped to be non-negative. Analogous to the Fourier basis for signals in \mathcal{R}^n , the lighting and irradiance can be written as a linear combination of spherical harmonics. The Funk-Hecke theorem is analogous to the convolution theorem, and tells us that for:

$$r = \sum_{l=0}^{\infty} \sum_{m=-l}^l r_l^m Y_l^m$$

we have

$$i = \sum_{l=0}^{\infty} \sum_{m=-l}^l i_l^m k_l^0 Y_l^m$$

Here Y_l^m denote the spherical harmonics. The index l indicates the order of the harmonic, corresponding to the frequency in the Fourier basis. Also, r_l^m are coefficients of the spherical harmonic transform of r , and k_l^0 are coefficients of the transform of the convolution kernel, which is a clipped cosine function. Since this is zonal, only coefficients with $m = 0$ are non-zero.

Table 9: AUC (%) of the model cross-type testing on CASIA-MFSD [63], Replay-Attack [10], and MSU-MFSD [49]

Method	CASIA-MFSD			Replay-Attack			MSU-MFSD			Overall
	Video	Cut Photo	Wrapped Photo	Video	Digital Photo	Printed Photo	Printed Photo	HR Video	Mobile Video	
DTN [28]	90.0	97.3	97.5	99.9	99.9	99.6	81.6	99.9	97.5	95.9±6.2
CDCN	98.48	99.90	99.80	100.00	99.43	99.92	70.82	100.00	99.99	96.48±9.64
CDCN++	98.07	99.90	99.60	99.98	99.89	99.98	72.29	100.00	99.98	96.63±9.15
SharinGAN + CDCN (Ours)	98.88	99.90	99.80	100.00	99.91	99.99	73.89	100.00	99.99	96.71±9.27

For distant lighting, [37] shows that $k_l^0 = 0$ for odd values of $l > 1$. For even values, k decays rapidly, and k_l^0 becomes quite small for $l > 2$. This implies that the image is largely determined by the first nine spherical harmonics of the lighting, of order 0, 1, and 2. When the lighting is not distant, [13] show that third order harmonics can also appear in i , but their effect becomes minimal when the light source is not very close to the object. For example, when the distance to the light is eight times the sphere’s radius, these effects become almost imperceptible.

Next, we consider the effect of light impinging on a printed photograph that is being imaged to create a spoof. We assume that the photo is matte (eg., Lambertian) and planar. If this is not the case, geometric distortion effects will provide further cues that can be used to detect a spoof. If the photograph is flat, and the light sources are distant, then the light’s intensity is completely uniform on the photo. The effect of light is merely to provide a scale factor to the resulting image. In this case, a photograph of a photograph will look identical to the original photograph, if it were captured with brighter or dimmer light.

If the light is not distant, then the intensity of light striking the photograph is generally not uniform. This effect does not drop off very quickly with the distance to the light. For example, if a source of light is at a 45° angle to the photograph, and the distance to it is eight times as large as half the width of the photo, the near side of the photograph will receive about 40% stronger illumination than the far side. In the supplementary material we consider the effects of the first order term in the variation of lighting on the photo.

Implications: While we analyze a simple sphere, it is clear that the geometric differences between a face and a sphere will only result in mapping a linear gradient in the image into a more complex variation in lighting on the face, creating potentially more higher order terms. To confirm the linear gradient in the images, we train a linear regressor between real images and spoof images. The linear regression input is the real image, and the output is the spoof image with the same identity. After learning this linear regressor, we multiply the spoof image by this gradient and retrain our RGB baseline on the OULU dataset (Protocol 1). We observe that the performance dropped from TPR@FPR=10-2 from 0.53 to 0.51, i.e. error rate for the RGB baseline increases by 3.4%. This shows that a linear gradient is present in OULU and that the baseline method makes use of it to

detect spoofs.

Our method of spoof detection makes use of SFSnet. The SFSnet is trained using a reconstruction loss based on a physical model that uses up to second-order harmonics to model lighting. Therefore, the SFSnet learns to push into the albedo components of the image that cannot arise from such lighting. Consequently, when a spoof is taken with a gradient of lighting on the photo that creates third-order harmonics, these will show up as artifacts in the albedo.

6. Conclusion

We propose to use albedo as a signal for PAD. We inferred that depth and normal maps are similar for spoof images and non-spoof images, while albedo is visually different. We show that albedo is a better cue for detecting spoofs as compared to normal. We add albedo as an additional signal to seven recent datasets and achieve state-of-the-art results on all of these datasets. We also show that contrast is being used as cue in existing methods, and removing it results in a drastic drop in performances. Finally, we provide theoretical analysis of how albedo can capture double lighting effects in the spoof images. Finally, we want to add that researchers should note that for the responsible development of this technology, it’s important to consider issues of potential unfair bias and consider testing for fairness.

7. Acknowledgments

This work is supported[, in part,] by the US Defense Advanced Research Projects Agency (DARPA) Semantic Forensics (SemaFor) Program under [award / grant / contract number] HR001120C0124. Any opinions, findings, and conclusions or recommendations expressed in this material are those of the author and do not necessarily reflect the views of the DARPA.

References

- [1] L. Ajjan, W. Jun, E. Sergio, H. J. Escalante, T. Zichang, Y. Qi, W. Kai, L. Chi, G. Guodong, G. Isabelle, and S. Z. Li. Multi-modal face anti-spoofing attack detection challenge at cvpr2019. In *Proceedings of the IEEE/CVF Conference on Computer Vision and Pattern Recognition (CVPR) Workshops*, June 2019.
- [2] I. Albuquerque, J. Monteiro, M. Darvishi, T. H. Falk, and I. Mitliagkas. Generalizing to unseen domains via distribution matching, 2020.

- [3] J. Amin, L. Yaojie, and L. Xiaoming. Face de-spoofing: Anti-spoofing via noise modeling. In *ECCV*, September 2018.
- [4] Y. Atoum, Y. Liu, A. Jourabloo, and X. Liu. Face anti-spoofing using patch and depth-based cnns. *2017 IEEE International Joint Conference on Biometrics (IJCB)*, pages 319–328, 2017.
- [5] V. Blanz and T. Vetter. A morphable model for the synthesis of 3d faces. In *SIGGRAPH '99*, 1999.
- [6] Z. Boulkenafet, J. Komulainen, and A. Hadid. Face anti-spoofing based on color texture analysis. *IEEE International Conference on Image Processing*, pages 2636–2640, 2015.
- [7] Z. Boulkenafet, J. Komulainen, and A. Hadid. face anti-spoofing based on color texture analysis, 2015.
- [8] Z. Boulkenafet, J. Komulainen, L. Li, X. Feng, and A. Hadid. OULU-NPU: A mobile face presentation attack database with real-world variations. May 2017.
- [9] T. Chen, S. Kornblith, M. Norouzi, and G. E. Hinton. A simple framework for contrastive learning of visual representations. *ArXiv*, abs/2002.05709, 2020.
- [10] I. Chingovska, A. Anjos, and S. Marcel. On the effectiveness of local binary patterns in face anti-spoofing. In *2012 BIOSIG - Proceedings of the International Conference of Biometrics Special Interest Group (BIOSIG)*, pages 1–7, 2012.
- [11] I. Chingovska, A. Anjos, and S. Marcel. On the effectiveness of local binary patterns in face anti-spoofing. *2012 BIOSIG - Proceedings of the International Conference of Biometrics Special Interest Group (BIOSIG)*, pages 1–7, 2012.
- [12] Y. Feng, F. Wu, X. Shao, Y. Wang, and X. Zhou. Joint 3d face reconstruction and dense alignment with position map regression network. In *ECCV*, 2018.
- [13] D. Frolova, D. Simakov, and R. Basri. Accuracy of spherical harmonic approximations for images of lambertian objects under far and near lighting. In *ECCV*, pages 574–587. Springer, 2004.
- [14] J. Gan, S. Li, Y. Zhai, and C. Liu. 3d convolutional neural network based on face anti-spoofing. *2017 2nd International Conference on Multimedia and Image Processing (ICMIP)*, pages 1–5, 2017.
- [15] K. Genova, F. Cole, A. Maschinot, A. Sarna, D. Vlasic, and W. Freeman. Unsupervised training for 3d morphable model regression. *CVPR*, pages 8377–8386, 2018.
- [16] A. George and S. Marcel. Deep pixel-wise binary supervision for face presentation attack detection. *2019 International Conference on Biometrics (ICB)*, pages 1–8, 2019.
- [17] K. He, H. Fan, Y. Wu, S. Xie, and R. B. Girshick. Momentum contrast for unsupervised visual representation learning. *CVPR*, pages 9726–9735, 2020.
- [18] O. J. Hénaff, A. Srinivas, J. Fauw, A. Razavi, C. Doersch, S. Eslami, and A. Oord. Data-efficient image recognition with contrastive predictive coding. *ArXiv*, abs/1905.09272, 2019.
- [19] Y. Jia, J. Zhang, S. Shan, and X. Chen. Single-side domain generalization for face anti-spoofing, 2020.
- [20] S. Joel, J. Amin, L. Yaojie, and L. Xiaoming. Noise modeling, synthesis and classification for generic object anti-spoofing. In *CVPR*, June 2020.
- [21] A. Jourabloo, Y. Liu, and X. Liu. Face de-spoofing: Anti-spoofing via noise modeling. In *ECCV*, 2018.
- [22] P. Khosla, P. Teterwak, C. Wang, A. Sarna, Y. Tian, P. Isola, A. Maschinot, L. Ce, and D. Krishnan. Supervised contrastive learning, 2020.
- [23] J. Komulainen, A. Hadid, and M. Pietikäinen. Context based face anti-spoofing. *2013 IEEE Sixth International Conference on Biometrics: Theory, Applications and Systems (BTAS)*, pages 1–8, 2013.
- [24] L. Kuang-Chih, H. Jeffrey, and K. D. J. Acquiring linear subspaces for face recognition under variable lighting. *IEEE Transactions on pattern analysis and machine intelligence*, 27(5):684–698, 2005.
- [25] S. Laine, T. Karras, T. Aila, A. Herva, S. Saito, R. Yu, H. Li, and J. Lehtinen. Production-level facial performance capture using deep convolutional neural networks. *Proceedings of the ACM SIGGRAPH / Eurographics Symposium on Computer Animation*, 2017.
- [26] Z. Lie and S. Dimitris. Face recognition under variable lighting using harmonic image exemplars. In *2003 IEEE Computer Society Conference on Computer Vision and Pattern Recognition, 2003. Proceedings.*, volume 1, pages I–I. IEEE, 2003.
- [27] F. Liu, L. Tran, and X. Liu. 3d face modeling from diverse raw scan data. *ICCV*, pages 9407–9417, 2019.
- [28] Y. Liu, J. Stehouwer, A. Jourabloo, and X. Liu. Deep tree learning for zero-shot face anti-spoofing, 2019.
- [29] D. Mahajan, S. Tople, and A. Sharma. Domain generalization using causal matching. *ArXiv*, abs/2006.07500, 2020.
- [30] M. Mancini, Z. Akata, E. Ricci, and B. Caputo. Towards recognizing unseen categories in unseen domains. In *ECCV*, 2020.
- [31] G. Pan, L. Sun, Z. Wu, and S. Lao. Eyeblink-based anti-spoofing in face recognition from a generic webcam. *2007 IEEE 11th International Conference on Computer Vision*, pages 1–8, 2007.
- [32] K. Patel, H. Han, and A. Jain. Secure face unlock: Spoof detection on smartphones. *IEEE Transactions on Information Forensics and Security*, 11:2268–2283, 2016.
- [33] B. Peixoto, C. Michelassi, and A. Rocha. Face liveness detection under bad illumination conditions. *2011 18th IEEE International Conference on Image Processing*, pages 3557–3560, 2011.
- [34] K. Pnvr, H. Zhou, and D. Jacobs. Sharingan: Combining synthetic and real data for unsupervised geometry estimation. *2020 (CVPR)*, pages 13971–13980, 2020.
- [35] Y. Qin, C. Zhao, X. Zhu, Z. Wang, Z. Yu, T. Fu, F. Zhou, J. Shi, and Z. Lei. Learning meta model for zero- and few-shot face anti-spoofing. In *AAAI*, 2020.
- [36] R. Ravi and H. Pat. An efficient representation for irradiance environment maps. In *Proceedings of the 28th annual conference on Computer graphics and interactive techniques*, pages 497–500, 2001.
- [37] B. Ronen and D. Jacobs. Lambertian reflectance and linear subspaces. *IEEE transactions on pattern analysis and machine intelligence*, 25(2):218–233, 2003.
- [38] S. Sengupta, A. Kanazawa, C. D. Castillo, and D. Jacobs. Sfsnet: Learning shape, reflectance and illuminance of faces 'in the wild'. *CVPR*, pages 6296–6305, 2018.
- [39] Z. Shu, E. Yumer, S. Hadap, K. Sunkavalli, E. Shechtman, and D. Samaras. Neural face editing with intrinsic image

- disentangling. (*CVPR*), pages 5444–5453, 2017.
- [40] T. A. Siddiqui, S. Bharadwaj, T. I. Dhamecha, A. Agarwal, M. Vatsa, R. Singh, and N. Ratha. Face anti-spoofing with multifeature videolet aggregation. *2016 23rd International Conference on Pattern Recognition (ICPR)*, pages 1035–1040, 2016.
- [41] M. Tappen, W. Freeman, and E. Adelson. Recovering intrinsic images from a single image. *IEEE Transactions on Pattern Analysis and Machine Intelligence*, 27:1459–1472, 2005.
- [42] A. Tewari, M. Zollhöfer, H. Kim, P. Garrido, F. Bernard, P. Pérez, and C. Theobalt. Mofa: Model-based deep convolutional face autoencoder for unsupervised monocular reconstruction. *2017 IEEE International Conference on Computer Vision Workshops (ICCVW)*, pages 1274–1283, 2017.
- [43] J. Thies, M. Zollhöfer, M. Stamminger, C. Theobalt, and M. Nießner. Face2face: real-time face capture and reenactment of rgb videos. *ArXiv*, abs/2007.14808, 2019.
- [44] A. Tran, T. Hassner, I. Masi, and G. Medioni. Regressing robust and discriminative 3d morphable models with a very deep neural network. *CVPR*, pages 1493–1502, 2017.
- [45] L. Tran and X. Liu. Nonlinear 3d face morphable model. *2018 IEEE/CVF Conference on Computer Vision and Pattern Recognition*, pages 7346–7355, 2018.
- [46] R. Volpi, H. Namkoong, O. Sener, J. C. Duchi, V. Murino, and S. Savarese. Generalizing to unseen domains via adversarial data augmentation. In *NeurIPS*, 2018.
- [47] A. Wagner, J. Wright, A. Ganesh, Z. Zhou, H. Mobahi, and Y. Ma. Toward a practical face recognition system: Robust alignment and illumination by sparse representation. *IEEE transactions on pattern analysis and machine intelligence*, 34(2):372–386, 2011.
- [48] Z. Wang, C. Zhao, Y. Qin, Q. Zhou, and Z. Lei. Exploiting temporal and depth information for multi-frame face anti-spoofing. *ArXiv*, abs/1811.05118, 2018.
- [49] D. Wen, H. Han, and A. K. Jain. Face spoof detection with image distortion analysis. *IEEE Transactions on Information Forensics and Security*, 10(4):746–761, 2015.
- [50] D. Wen, H. Han, and A. K. Jain. Face spoof detection with image distortion analysis. *IEEE Transactions on Information Forensics and Security*, 10:746–761, 2015.
- [51] X. Chen, H. Fan, R. B. Girshick, and K. He. Improved baselines with momentum contrastive learning. *ArXiv*, abs/2003.04297, 2020.
- [52] X. Yang, W. Luo, L. Bao, Y. Gao, D. Gong, S. Zheng, Z. Li, and W. Liu. Face anti-spoofing: Model matters, so does data. (*CVPR*), pages 3502–3511, 2019.
- [53] Z. Yu, Y. Qin, X. Li, Z. Wang, C. Zhao, Z. Lei, and G. Zhao. Multi-modal face anti-spoofing based on central difference networks. *CVPR Workshop*, pages 2766–2774, 2020.
- [54] Z. Yu, Y. Qin, X. Xu, C. Zhao, Z. Wang, Z. Lei, and G. Zhao. Auto-fas: Searching lightweight networks for face anti-spoofing. *ICASSP 2020 - 2020 IEEE International Conference on Acoustics, Speech and Signal Processing (ICASSP)*, pages 996–1000, 2020.
- [55] Z. Yu, J. Wan, Y. Qin, X. Li, S. Li, and G. Zhao. Nas-fas: Static-dynamic central difference network search for face anti-spoofing. *IEEE Transactions on Pattern Analysis and Machine Intelligence*, 43:3005–3023, 2021.
- [56] Z. Yuanhan, Y. Zhenfei, L. Yidong, Y. Guojun, Y. Junjie, S. Jing, and L. Ziwei. Celeba-spoof: Large-scale face anti-spoofing dataset with rich annotations. In *ECCV*, 2020.
- [57] Q. Yunxiao, Z. Chenxu, Z. Xiangyu, W. Zezheng, Y. Zitong, F. Tianyu, Z. Feng, S. Jingping, and L. Zhen. Learning meta model for zero-and few-shot face anti-spoofing. In *AAAI*, 2020.
- [58] W. Zezheng, Y. Zitong, Z. Chenxu, Z. Xiangyu, Q. Yunxiao, Z. Qiusheng, Z. Feng, and L. Zhen. Deep spatial gradient and temporal depth learning for face anti-spoofing. In *CVPR*, 2020.
- [59] W. Zezheng, Y. Zitong, Z. Chenxu, Z. Xiangyu, Q. Yunxiao, Q. Zhou, Z. Feng, and L. Zhen. Deep spatial gradient and temporal depth learning for face anti-spoofing. In *CVPR*, June 2020.
- [60] K. Zhang, T. Yao, J. Zhang, Y. Tai, S. Ding, J. Li, F. Huang, H. Song, and L. Ma. Face anti-spoofing via disentangled representation learning. *ArXiv*, abs/2008.08250, 2020.
- [61] S. Zhang, A. Liu, J. Wan, Y. Liang, G. Guo, S. Escalera, J. Escalante, and L. S. Z. Casia-surf: A large-scale multi-modal benchmark for face anti-spoofing, 2020.
- [62] Z. Zhang, J. Yan, S. Liu, Z. Lei, D. Yi, and S. Li. A face antispoofing database with diverse attacks. *2012 5th IAPR International Conference on Biometrics (ICB)*, pages 26–31, 2012.
- [63] Z. Zhang, J. Yan, S. Liu, Z. Lei, D. Yi, and S. Z. Li. A face antispoofing database with diverse attacks. In *2012 5th IAPR International Conference on Biometrics (ICB)*, pages 26–31, 2012.
- [64] X. Zhu, H. Wang, H. Fei, Z. Lei, and S. Z. Li. Face forgery detection by 3d decomposition. In *Proceedings of the IEEE/CVF Conference on Computer Vision and Pattern Recognition (CVPR)*, pages 2929–2939, June 2021.
- [65] Y. Zitong, Z. Chenxu, W. Zezheng, Q. Yunxiao, S. Zhuo, L. Xiaobai, Z. Feng, and Z. Guoying. Searching central difference convolutional networks for face anti-spoofing. In *CVPR*, 2020.
- [66] Y. Zitong, Q. Yunxiao, L. Xiaobai, W. Zezheng, Z. Chenxu, L. Zhen, and Z. Guoying. Multi-modal face anti-spoofing based on central difference networks. In *CVPR Workshop*, 2020.
- [67] L. Ziwei, L. Ping, W. Xiaogang, and T. Xiaoou. Deep learning face attributes in the wild. In (*ICCV*), December 2015.